5. OPTIONS FOR PLASMA REGIMES OF OPERATION

Stephen C. Jardin
Charles E. Kessel, Jr.
Tak-Kuen Mau
BongJu Lee
David A. Ehst
Charles G. Bathke

Contents

5.1. INTRODUCTION 5-1

5.2. PHYSICS FIGURES OF MERIT 5-3

5.2.1. MHD Stability 5-3

5.2.2. Current Drive 5-7

5.2.3. Energy Confinement 5-11

5.2.4. Heat Exhaust 5-16

5.2.5. Helium Ash Removal 5-18

5.3. CONCEPT EVALUATION 5-23

5.3.1. First Stability [ARIES-I] 5-23

5.3.2. Pulsed Operation [PULSAR] 5-25

5.3.3. Second Stability [ARIES-II/IV] 5-25

5.3.4. Reversed Shear 5-26

5.3.5. Low-Aspect-Ratio 5-26

5.4. Starlite Reference Design 5-27

5.5. SUMMARY AND CONCLUSIONS 5-28

REFERENCES 5-31

5. OPTIONS FOR PLASMA REGIMES OF OPERATION

5.1. INTRODUCTION

The Starlite project aims at developing the most attractive and credible conceptual design for a fusion power plant, based on the physics understanding and experimental data established to date. This design will utilize the tokamak magnetic confinement concept, which has emerged as the clear concept-of-choice in the worldwide fusion program. However, there are at least five distinctly different tokamak operating modes that have been proposed for utilization in a D–T-fueled tokamak power plant. These five operating modes differ from one another in one or more of the following areas: (i) choice of stability regime (*i.e.,* first regime, second regime, or mixed), (ii) choice of pulsed or steady state operation, and (iii) choice of conventional or low aspect ratio. While each of the five operating modes leads to a self-consistent design that is optimized within its unique set of design constraints, the five modes optimize to very different plasma performance and engineering requirements, and hence, a choice must be made among them.

The five tokamak operating modes that have been evaluated by the Starlite project are: (1) a steady state, first stability regime (FS) similar to ARIES-I [1]; (2) a pulsed, first stability regime (PU) similar to PULSAR [2]; (3) a steady state, second stability (SS) regime similar to ARIES-II/IV [3]; (4) a steady state, reversed shear (RS) mode [4]; and (5) a steady state, low aspect ratio configuration [5]. Each of the five operating modes has a substantial theoretical basis involving the computation of self-consistent ideal MHD equilibrium and stability, bootstrap current, and current-drive efficiency. However, not all of the five modes have been experimentally prototyped to the same degree.

We have identified a set of critical tokamak physics parameters called physics Figures of Merit (FOM). Comparing the FOM parameters for each of the five operating modes with what have actually been obtained experimentally provides a way of assessing how credible the different tokamak operating modes are [6]. For example, if there are two operating modes that lead to approximately the same cost of electricity (COE) projections, but one is significantly closer to having been experimentally prototyped in each of the key tokamak physics areas, then that one operating mode would clearly be preferred as a design choice.

In the remainder of this chapter, we define and motivate the FOM parameters in each of the critical tokamak physics areas (Sec. 5.2), summarize each of the five tokamak operating mode concepts(Sec. 5.3), present figures comparing the five concepts with the tokamak data base that has been assembled for ITER(Sec. 5.5), and present arguments for why the reversed shear (RS) operating mode appears to be the most attractive one at this time. A chart illustrating the relationship between the physics, technology, and economic assessments of the concepts and the project mission and requirements statements is shown in Fig. 5.1-1.

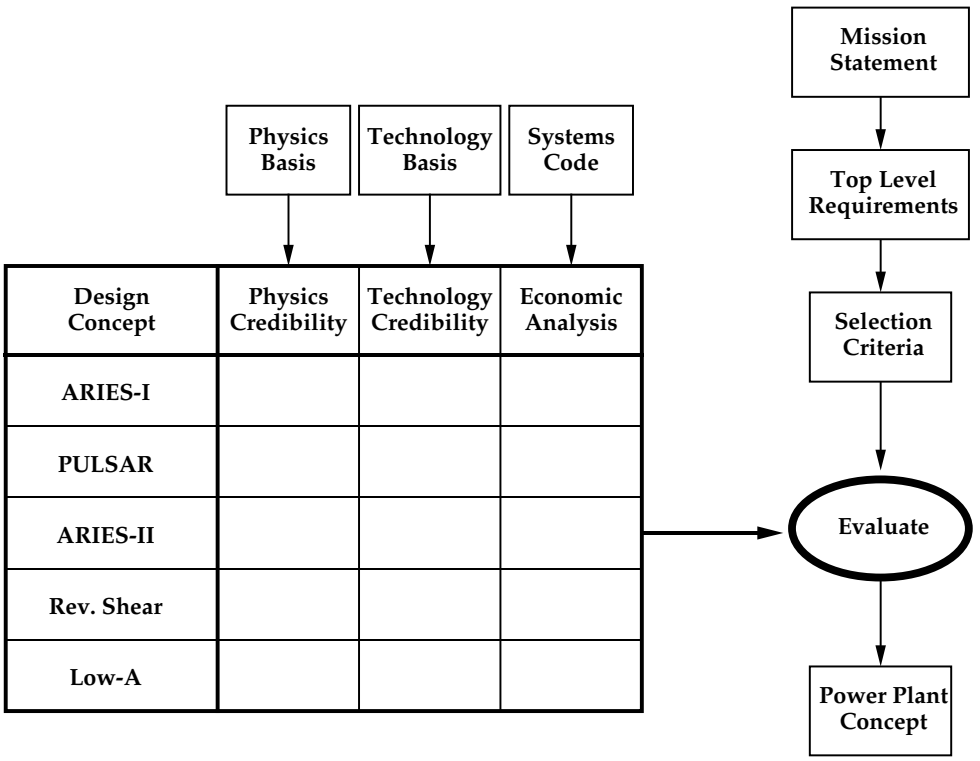

Figure 5.1-1. Flowchart showing strategy for Starlite fusion power plant evaluation.

5.2. PHYSICS FIGURES OF MERIT

The performance properties and hence the economics of the power plant will be largely determined by the baseline tokamak physics parameters. These are significantly different for each of the five candidate designs. For the power plant to be both economically attractive and physically credible, several of these parameters must be at or near their allowable limits, but none may exceed them. In an attempt to quantify this and to aid in concept selection, five critical areas of tokamak physics have been identified. In each of these areas, we have further identified one or more critical parameters, or figures of merit (FOM), which are dimensionless (wherever possible) measures of how close to the theoretical limits a tokamak can be operated. Before the detailed engineering design can proceed, there must be sufficient experimental data in place to demonstrate that a tokamak can operate reliably with the design values of the FOMs in the five critical areas. Thus, by comparing the FOMs of the five candidate designs with the existing tokamak data base we can determine the relative credibility of the five designs. In addition, identification of these critical parameters should help focus present research efforts in the direction of optimizing and improving these quantities in existing and planned experiments in order to lead the way to a more attractive concept. The five critical physics areas are (A) MHD stability, (B) current drive, (C) plasma energy confinement, (D) power exhaust, and (E) helium ash removal. The relevant FOMs are discussed in the following subsections.

5.2.1. MHD Stability

There are advantages to operating a tokamak at high values of β/ϵ to achieve high fusion power density, p_f, and at high values of $\epsilon\beta_p$ to achieve a high bootstrap current fraction, and consequently low recirculating power. Here plasma β is defined as $2\mu_o\langle p\rangle/B_T^2$ and the poloidal β given by $\beta_p \equiv 8\pi^2 a_p^2\langle p\rangle S/\mu_o I_p^2$, where $\langle p\rangle$ denotes the volume averaged pressure, B_T is the toroidal field in vacuum at the plasma major radius R, I_p is the total plasma current, $S \equiv (1+\kappa^2)/2$ is the shape factor , $\epsilon \equiv A^{-1} \equiv a_p/R$ is the inverse aspect ratio, a_p is the minor radius, and κ is the elongation. Another useful quantity that will be used in this subsection is the circularized safety factor, $q_* \equiv 2\pi a_p^2 B_T S/\mu_o R I_p$.

It should be noted that β/ϵ, and not β, is a parameter of fundamental importance. It is well known that if the MHD equilibrium and stability equations are expanded in a self-consistent inverse-aspect-ratio ordering that allows pressure driven instabilities to be present, the so-called high-β ordering [7], then the tokamak β is of order ϵ and the β_p is

of order ϵ^{-1}. Thus, to leading order in the expansion parameter ϵ, the equilibrium and stability properties of a high-β tokamak configuration depend only on β/ϵ and on $\epsilon\beta_p$.

Furthermore, it follows that β/ϵ is the critical parameter if one assumes that p_f scales as $\beta^2 B_T^4$, and that the limiting value of B_T scales like $\epsilon^{-1/2}$. This scaling for the maximum field strength at the plasma center comes from assuming that in a tokamak power plant, the maximum toroidal field will be limited by the requirement that the maximum field strength at the superconducting TF coil is below some critical value, B_{crit}. Assuming that the outermost part of the inside leg of the TF coil and the inside edge of the plasma are separated by shielding, etc, which occupies about 20% of the major radius, leads to a dependence of field strength on inverse aspect ratio which is very well approximated by $\epsilon^{-1/2}$ for the range of aspect ratios: $2.5 \leq A \leq 5$.

It is cautioned in passing that profile effects that affect the fusion power density have been ignored. The true fusion power output from a D–T plasma would be better approximated by $\langle p^2 \rangle$ than by $\langle p \rangle^2$ as has been done here. The latter quantity has been chosen for the simplifications it yields, and for its ease of measurement in existing experiments. However, care must be used in applying the results discussed here to tokamak equilibria with extreme ratios of $\langle p^2 \rangle$ to $\langle p \rangle^2$.

Increasing $\epsilon\beta_p$ in a given tokamak will normally increase its ratio of toroidal current driven by the bootstrap effect to the total current, $f_{BS} \equiv I_{BS}/I_p$. However, the bootstrap fraction actually scales as $f_{BS} \propto C_{BS}\epsilon\beta_p/\sqrt{\epsilon}$ [8], where C_{BS} contains dependences on current, density, and temperature profiles. The factor $\sqrt{\epsilon}$ reflects the decrease in bootstrap current as the aspect ratio is reduced.

There are limits on how much β/ϵ and $\epsilon\beta_p$ can be increased, either separately or together. These constraints can be conveniently illustrated in a diagram plotting $\beta/(\epsilon S)$ vs $\epsilon\beta_p$, as is displayed in Fig. 5.2-1. The beta limit, in the form $\beta \leq \beta_N(I_p/B_T a_p)$, can be shown to be equivalent to the expression

$$(\epsilon\beta_p)\left(\frac{\beta}{\epsilon}\right) \;\leq\; \left(\frac{\beta_N}{20}\right)^2 S\,, \tag{5.2-1}$$

which is plotted in Fig. 5.2-1 for two values of β_N. For a conventional first stability configuration (similar to PULSAR) with high current (low q_*), optimally shaped current and pressure distributions, and with sufficient triangularity in the cross-sectional shape, this equation must be obeyed with a Troyon coefficient of $\beta_N = 3.5$. Plasma configurations with non-optimal profiles and shapes can be unstable at values of β_N lower than 3.5. If a higher f_{BS} is desired for steady state operation, one can reduce the current or raise q_*, resulting in a lower β, as is the case with ARIES-I.

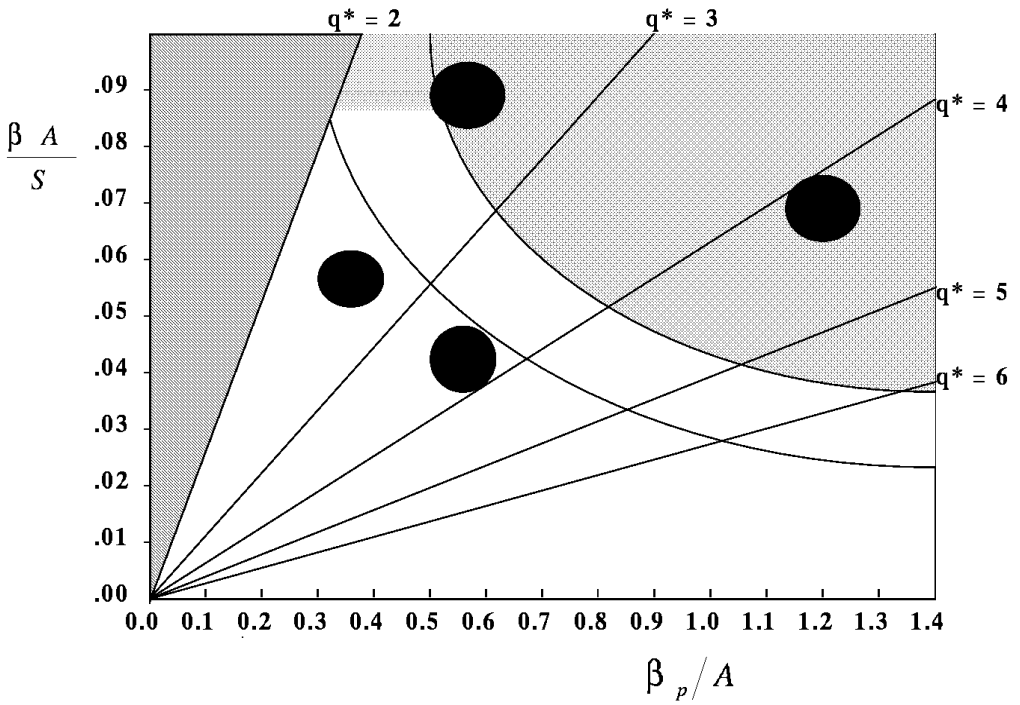

Figure 5.2-1. The MHD stability diagram showing regimes of operation for the first-stabilty (FS), pulsed-plasma (PU), reversed-shear (RS), and second-stabtility (SS) Starlite power plant options. The LAR regime is outside of this diagram, with $\epsilon\beta_p \sim 1$.

It may be possible to violate the Troyon limit if certain conditions are met which allow second stability regime as in ARIES-II/IV designs, or at very large values of q_* [9] or at very low aspect ratios [10]. The conditions which allow second stability include either elevated central safety factor ($q_0 \geq 2$) [11], strong cross-sectional indentation [12], or reversed magnetic shear [4]. In addition to these requirements, stabilization of the external kink mode in a second stability plasma requires a close fitting conducting wall and sufficient plasma rotation [13].

Other constraints, also shown in Fig. 5.2-1, come from the fact that the equilibrium equation must be obeyed, which implies $\epsilon\beta_p \leq 2$ and that the external kink mode can only be stable for $q_* \geq 2$. The expression relating these quantities for a plasma equilibrium is

$$\left(\frac{\beta}{\epsilon}\right) \;=\; (\epsilon\beta_p)\,\frac{S}{q_*^2} \tag{5.2-2}$$

which appears as straight lines in Fig. 5.2-1.

It is natural to choose as the MHD figures of merit the parameter pair $(\beta/\epsilon, \epsilon\beta_p)$. Note that a systems analysis is required to choose where in this space the fusion power plant should operate. There will always be a tradeoff between high $\epsilon\beta_p$ and high β/ϵ as described by Eq. (5.2-1), and the preferred design will most likely optimize at intermediate values of each as is in all ARIES designs. An explicit illustration of the tradeoff between high β and high β_p is given in Ref. [14], in which an economic analysis determines the values of these parameters that minimize the COE of a first stability equilibrium with an ARIES-I type of current drive performance.

Existing long-pulse, ELMy H-mode discharges with high β and high bootstrap fraction are plotted in the two-dimensional parameter space of Fig. 5.2-2, together with the design values for the five Starlite power plant options. This figure allows one to assess how close a proposed tokamak power plant is to the existing MHD database. In this respect, both the FS and PU concepts are close to the database. Several caveats must be kept in

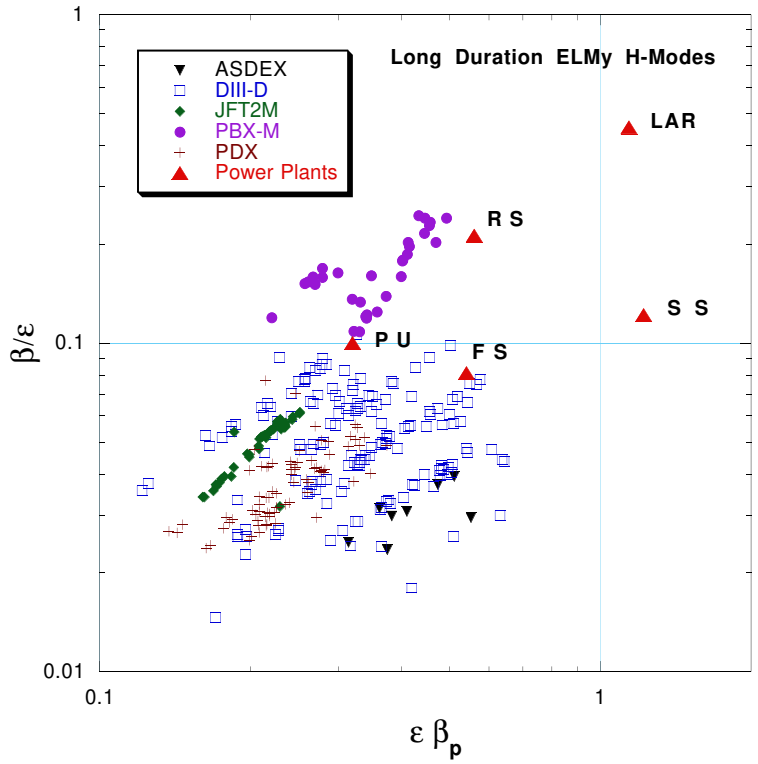

Figure 5.2-2. MHD figures of merit for long-pulse ELMy, H-mode discharges in several existing devices and the five Starlite fusion power plant options (FS, PU, RS, SS, and LAR).

mind, however. One is that the PBX-M data are based on highly indented plasmas ($i \simeq 0.25$), which do not extrapolate well to power plant regimes. The second is that the nature of MHD changes at very high temperatures, transitioning from a resistive to a collisionless regime. This fact makes the lower temperature results in smaller, colder, present day experiments not completely relevant for prototyping the MHD regimes in a burning plasma. Another caveat is that the MHD time-scales needed for plasma profiles to fully relax and for weakly unstable dissipative MHD instabilities to grow can be very long by today's standards, so that few if any of the discharges displayed in Fig. 5.2-2 are truly in steady state.

5.2.2. Current Drive

The theory for non-inductive current drive [15–17] demonstrates that the driven current density, j_{cd}, is proportional to the product of the local absorbed power density, p_{cd}, and the local electron temperature, T_e, divided by the electron density,

$$j_{cd} \;=\; A_0\, p_{cd}\, \frac{T_e}{n_e} \left(\frac{\tilde{j}}{\tilde{p}}\right) . \tag{5.2-3}$$

Here A_0 is a constant. The normalized local current drive efficiency $(\tilde{j}/\tilde{p})$ (defined in [15]) is a dimensionless function of the location in electron velocity space where momentum and energy are absorbed. In a steady state plasma with no applied loop voltage, the total non-inductively driven current, I_{CD}, is found by integrating the local driven current density, j_{cd}, over the plasma cross section. Including the Pfirsch-Schlüter and diamagnetic equilibrium contributions, the total driven current is of the form

$$I_{CD} \;=\; \gamma_{CD} \left(\frac{P_{CD}}{\overline{n}_e R}\right) , \tag{5.2-4}$$

which may also be obtained by dimensional analysis [18]). Reference to Eq. (5.2-3) shows roughly that $\gamma_{CD} \sim T_e(\tilde{j}/\tilde{p})$. Detailed calculations of self-consistent steady state tokamaks [16] have refined the temperature dependence for a power plant ($T_{e0} \geq 15$ keV) to $\gamma_{CD} \propto T_{e0}^n$, where $0.6 \leq n \leq 0.8$, depending on details of the plasma and current density profiles.

Because the current-drive efficiency for most of the established current-drive techniques is low, steady-state tokamak power plants have to rely heavily on the bootstrap current. For a high β_p tokamak plasma, the toroidal plasma current, I_p, consists of two components, one generated by one or more non-inductive current-drive sources with

power P_{CD}, and the other due to the toroidal bootstrap effect, *i.e.,* $I_p = I_{BS} + I_{CD}$. To account for these two factors, a more appropriate, bootstrap-enhanced current-drive figure of merit, γ_B, is proposed, which is the same as the conventional measure of current-drive efficiency (γ_{CD}) but with I_{CD} replaced by I_p, and is given by

$$\gamma_B \;=\; (\overline{n}_e/10^{20}) I_p R/P_{CD}\,. \tag{5.2-5}$$

The expression γ_B can be viewed as a global integral of the current-drive efficiency over the plasma minor cross section, including the bootstrap contribution. Thus, to lowest order, γ_B depends on the plasma equilibrium and on the electron temperature, T_e; to next order, it depends on details such as current drive techniques, plasma Z_{eff}, and equilibrium T_e and n_e profiles. It is clear from Eq. (5.2-5) that γ_B can be made large if a large part of I_p is due to the bootstrap effect, *i.e.,* if $f_{BS} \equiv I_{BS}/I_p$ is close to unity. In recent years, significant advances have been made in achieving high bootstrap current fraction in high-β_p experimental discharges, and Fig. 5.2-3 illustrates some of the results. As shown in this figure, f_{BS} values close to 0.8 have been obtained.

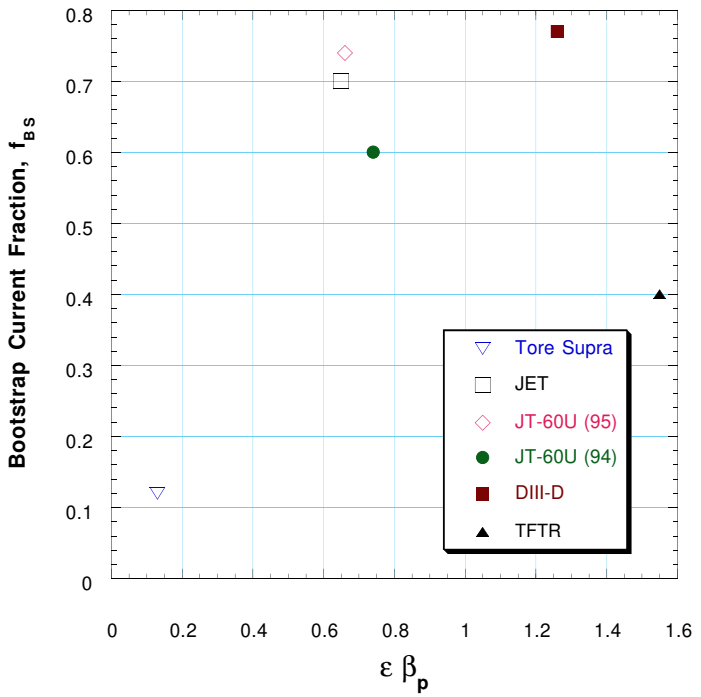

Figure 5.2-3. Large tokamak experiments which display substantial bootstrap fraction at high poloidal beta. Note that poloidal beta definitions vary somewhat; and plasma conditions (collisionality, density gradient, impurity content, *etc.*) also vary.

For steady-state tokamak power plants, various non-inductive techniques need to be considered for sustaining the plasma current (*i.e.,* the supply the difference between the bootstrap and equilibrium plasma currents). Depending on the reference equilibrium, a combination of these techniques may be required to drive currents in different locations within the plasma. The bulk of the present experimental database on current drive has been obtained using lower hybrid waves and neutral beams. In these discharges, typically $f_{BS} \leq 0.1$, so that $\gamma_B \simeq \gamma_{CD}$. Figure 5.2-4 shows the experimental values of the current-drive efficiency as a function of central electron temperature, T_{e0} for lower hybrid current drive (LHCD) [19], the measured values lying within the expected range of $\tilde{j}/\tilde{p}$. With lower hybrid power alone, the highest value of $\gamma_{CD} = 0.34$, measured on JT-60 [20], is displayed in the figure.

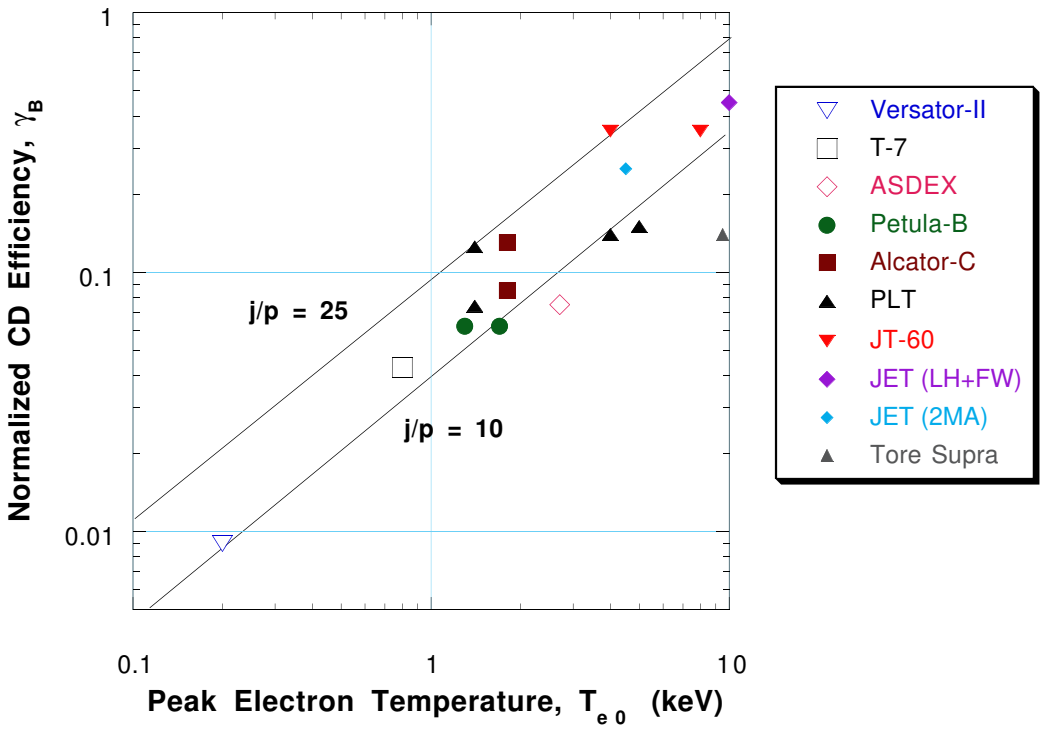

Figure 5.2-4. Experimental values of the lower-hybrid current-drive efficiency as a function of central electron temperature, T_{e0}; for most of these experiments the bootstrap current contribution is small so $\gamma_B \simeq \gamma_{CD}$.

There are two other current-drive techniques, namely, fast magnetosonic waves in the ion cyclotron range of frequencies (ICRF) and electron cyclotron waves, that exhibit potentials for power plant applications. The fast wave technique shows significant promise for on-axis current drive, particularly in view of the fact that a typical fusion plasma core is inaccessible to the lower-hybrid waves. In Fig. 5.2-5 the most recent experimental data on ICRF fast-wave current drive (FWCD) are plotted. Most of these data points come from DIII-D [21], where the plasma was preheated either by electron-cyclotron waves or by neutral beam injection, and where a four-strap directional antenna is used. Preliminary FWCD data taken at Tore-Supra [22] and TFTR [23] are displayed alongside the DIII-D data, and were obtained with two-strap 90° phased antennas in preheated plasmas. Also shown in this figure is the record value of $\gamma_{CD} = 0.45$ achieved to date on JET [24], when a synergistic combination of lower-hybrid and ICRF power was used. For reference and comparison, the highest γ_B value of 0.34, achieved on JT-60 using lower-hybrid power alone [20], is also displayed.

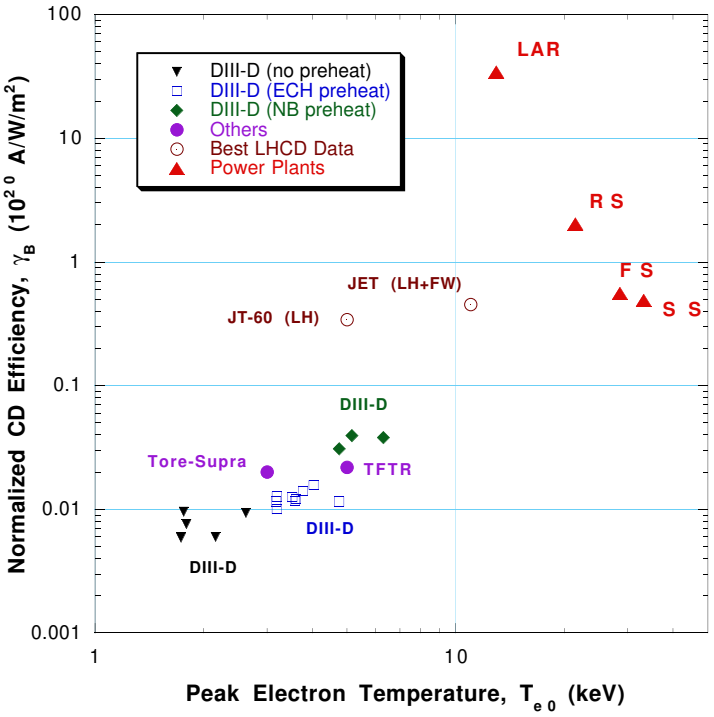

Figure 5.2-5. Fast-wave current-drive experimental database on DIII-D [21], Tore Supra [22], and TFTR [23]; best data point for lower-hybrid current-drive on JT-60 [20] and for lower-hybrid and FWCD synergy on JET [24]. Reference γ_B values for Starlite power plant options (FS, PU, RS, SS, and LAR) are also shown.

In Fig. 5.2-5, the design values of γ_B (using a combination of RF techniques) for the FS, SS, RS, and LAR power plant options are also shown. These design points are at much higher values of T_{e0} than in present experiments. It is clear that considerable advances in the current-drive database with FWCD are required in order to reach the power plant regime. However, as the target plasma temperature improves with higher input power, and as the bootstrap fraction is raised in future devices, the value of the measured γ_B is expected to increase accordingly.

It should be noted that the current-drive data quoted so far have all been taken in transient discharges, with the driven current deduced either from loop-voltage measurements or from comparison between co- and counter-current drive discharges. The only truly steady state discharge to date was achieved on TRIAM-1M [25], where lower-hybrid current-drive was used to maintain the discharge at $I_p \sim 22$ kA for over one hour, which well exceeds the current profile relaxation time. However, the plasma parameters were modest, with $\langle n_e \rangle < 0.2 \times 10^{19}$ m^{-3}, and an input lower-hybrid power of 50 kW.

More recently, a completely non-inductively-driven quasi-stationary state of 0.1 s duration was achieved during a transient DIII-D discharge when 1.5MW of FWCD and 1.0 MW of electron-cyclotron current-drive (ECCD) were injected [21]. During this period, the plasma current was held constant at 170 kA by a standard feedback control of the loop voltage that stayed approximately near zero. Detailed calculations showed that the FWCD, ECCD and bootstrap effect account for 100, 10, and 60 kA, respectively. In spite of these advances, it remains clear that database need to be developed for long pulse and steady state discharges with the use of non-inductive current drive.

5.2.3. Energy Confinement

Plasma energy confinement is one of the most important issues for a fusion power plant design, but is not yet well understood. It is measured by the global energy confinement time, τ_E, which is defined as the time for the transport of plasma energy across the confining magnetic field, from the core to the edge region. From a single particle orbit perspective, the value of τ_E depends intrinsically on the size of the toroidal plasma, and on the magnitude of the confining magnetic field. However, the actual level of energy confinement is governed by the detailed transport processes induced by drift wave turbulence and microinstabilities due to various plasma gradients and the presence of magnetically trapped particles. As a result, the tokamak plasma can exhibit a variety of confinement modes.

There are two classes of plasma confinement regimes in tokamak discharges that involve auxiliary heating power. The first class includes L-mode discharges where the energy confinement is low and where no attempt is made to improve the confinement by external means. The second class includes regimes with enhanced confinement (quiet H-mode, ELMy H-mode, Supershot, PEP H-mode, high-β_p H-mode, VH-mode, enhanced reversed shear mode, *etc.*). In general, better energy confinement, together with higher normalized β lead to a more compact, and potentially more economical fusion power core, limited only by the allowable magnetic field at the toroidal-field coils, neutron wall loading, *etc.*and MHD stability limits. In a fusion power plant, the plasma will have to operate in one of these enhanced confinement regimes to be viable.

Among the various energy confinement regimes, L-mode discharges have been studied most extensively. As part of the ITER Conceptual Design Activities, an empirical τ_E scaling [33] was obtained from a large number of tokamak L-mode discharges with different heating methods (neutral beam and RF) and different exhaust configurations (divertor and limiter), using an ordinary least squares regression technique. This confinement time scaling is given by

$$\tau_{ITER89-P} \;=\; 0.048\, I_p^{0.85}\, R^{1.2}\, a_p^{0.3}\, \kappa^{0.5}\, \bar{n}_{20}^{0.1}\, B^{0.2}\, A_i^{0.5}\, P^{-0.5}\,, \qquad (5.2\text{-}6)$$

where A_i is the ion mass number, and SI units are used except for plasma current I_p (MA), total heating power, P (MW), and the line-averaged electron density $\bar{n}_{20}$ ($10^{20}/m^3$).

On the other hand, except for the quiet and ELMy H-modes, confinement scalings for the enhanced confinement regimes of operation have yet to be established. This is partly because of an insufficient database and partly because many of these discharges rely on detailed control of the plasma profiles that may require a new methodology to parameterize. The reference ITER plasma operational regimes [34] will be based on the ELMy H-mode confinement regime in order to ensure ignition with a modest heating power requirement and moderate ash buildup in the plasma. However, unlike ITER which has a relatively conservative near-term goal, selection of the power plant operation scenario will require the consideration of a much broader range of enhanced confinement modes in order to maximize its economic potential.

An important consideration for ignition devices (such as ITER) and fusion power plants is the plasma pressure $\langle p \rangle \equiv \langle nT \rangle$ at which these enhanced confinement modes are achieved. For ion temperatures in the range of 5–25 keV, typical of a D–T-burning plasma, the fusion power is proportional to $\langle nT \rangle^2$. Using simple power balance, the ratio of fusion power to the rate at which energy is conducted away is proportional to $\langle nT \rangle \tau_E$, which more appropriately characterizes the confinement capacity for a fusion plasma than

τ_E alone. As an example, the ITER-CDA device will require a confinement capacity of $T_{i0} n_{DT0} \tau_E \sim 4 - 8 \times 10^{21}$ keV·s/m^3 for a fusion $Q \sim 5 - \infty$. Using $\langle nT \rangle \sim \beta B_T^2$ and $\chi_E \sim a_p^2/\tau_E$, where χ_E is a volume averaged heat diffusivity, one can obtain:

$$\frac{\beta}{\chi_E} \sim \frac{\beta\,\tau_E}{a_p^2} \sim \frac{\langle nT \rangle \tau_E}{(a_p B_T)^2}\,. \tag{5.2-7}$$

Note that in Eq. 5.2-7, the quantity $\beta\tau_E/a_p^2$ provides a normalized measure of the confinement capacity, by factoring out the dominant dependences of the device size and magnetic field. This parameter is also proportional to β/χ_E, which was previously proposed as a power-plant figure of merit [35].

Another commonly used figure of merit for confinement capacity can be derived from the quantity $\langle nT \rangle \tau_E$, irrespective of machine size and easily measurable in present experiments. By invoking a "generic" L/H-mode scaling [36] of $\tau_E \propto H I_p R^{3/2} \kappa^{1/2} P^{-1/2}$, and noting that $P \propto (\langle nT \rangle / \tau_E) R a_p^2 \kappa$, one can derive the relation $\langle nT \rangle \tau_E \propto (H I_p/\epsilon)^2$, where H is the H-mode confinement enhancement factor. Neglecting shape factors (δ, κ) and substituting $q_* \propto \epsilon a_p B_T / I_p$ into the above expression yields the relationship

$$\frac{\langle nT \rangle \tau_E}{(a_p B_T)^2} \propto \left(\frac{H}{q_*}\right)^2\,, \tag{5.2-8}$$

denoting that H/q_* as a figure of merit. However, the derivation of this figure of merit depends on the "generic" L/H-mode scaling. Recently, the ITER H-mode Database Working Group derived global confinement scalings from various subsets of the H-mode confinement database and found that the parameter exponents can differ substantially from those of the ITER-89P L-mode scaling. For example, for ELMy H-modes, the thermal energy confinement scaling is found to be [37]:

$$\tau_{H-mode} = 0.045\, I_p^{1.06}\, R^{1.79}\, \kappa^{0.66}\, \bar{n}_{20}^{0.17}\, B_T^{0.32}\, A_i^{0.41}\, P^{-0.67}\, \epsilon^{-0.11}\,, \tag{5.2-9}$$

where P is now the total heating power corrected for beam shine-through, orbit loss and charge exchange losses. Comparing Eqs. 5.2-6 and 5.2-9 illustrates that there is substantial variation from the "generic" L/H-mode scaling and that the use of H/q_* as a figure of merit is not universally applicable.

Since, the cost of operating a fusion power plant is strongly dependent on the achievable fusion power density, we propose plotting the confinement figure of merit $\beta\tau_E/a_p^2$ as a function of β/ϵ.[1] Simultaneous attainment of high confinement capacity and high

[1] This combination was first proposed by R. Goldston, PPPL(1994).

fusion power density will then place the desirable region of operation in the upper right-hand quadrant of such a graph. This also serves as a guide to present and near-term experiments aimed at simulating attractive reactor confinement performance.

In Fig. 5.2-6, taken from Ref. [36], values of $\beta\tau_E/a_p^2$ is plotted against $(\beta/\epsilon)^2$ for ELM-free H-modes on DIII-D, and for a number of existing and future devices, including JET, JT-60U, TPX and ITER. The DIII-D data are plotted for various combinations of triangularity (δ) and elongation (κ), clearly indicating that energy confinement and energy density improve significantly with strong plasma shaping.

Since ELMs are useful in periodically removing the α ash from the core, it is useful to compare the ELMy H-mode database with power plant values. In Fig. 5.2-7 the confinement FOMs are plotted for long pulse ELMy H-mode discharges on a number of devices together with the reference values for the five Starlite power plants. Note that the very favorable results for PBX-M are due to the highly indented plasma ($i \sim 0.25$) in those discharges. In general, the FOM values are more modest than those for ELM-free

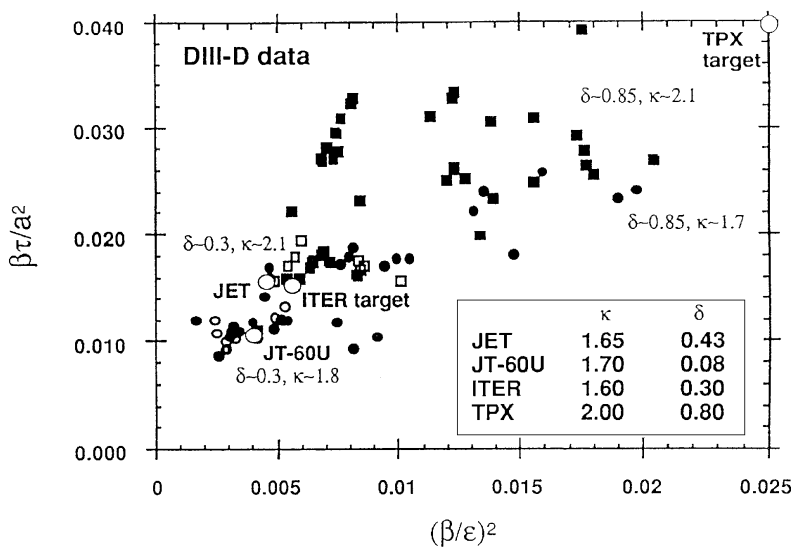

Figure 5.2-6. Energy confinement figures of merit for ELM-free H-mode discharges on DIII-D for various (δ, κ) values. Data points for JET, JT-60U, and design values for TPX and ITER are also displayed. [36]

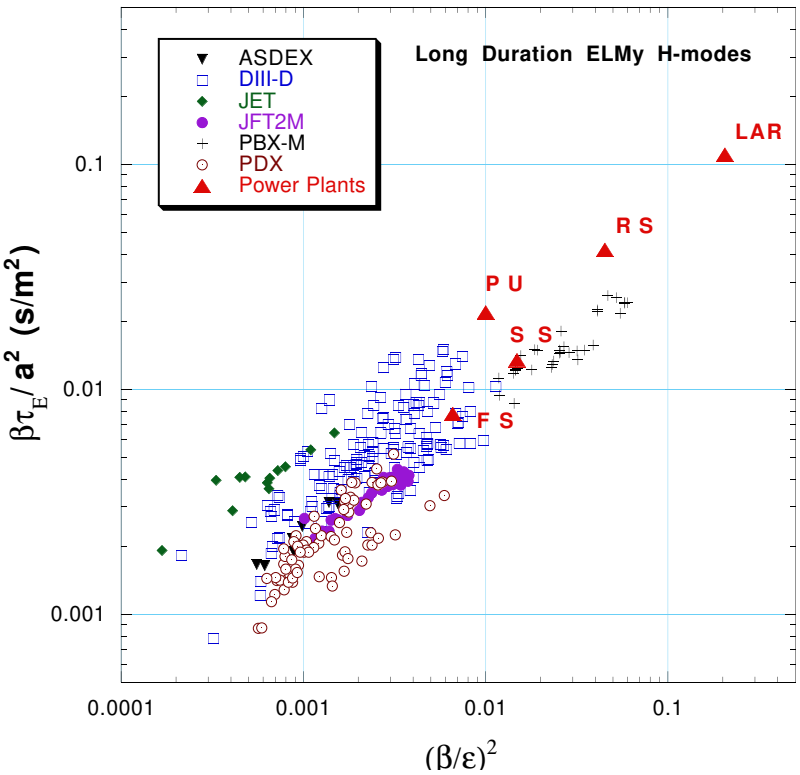

Figure 5.2-7. Energy confinement figures of merit for a number existing tokamaks and the Starlite fusion power plants. (Data provided by Stan Kaye, PPPL.)

discharges shown in Fig. 5.2-6. As indicated, the confinement performance of the FS option is well within those achieved on present machines, while the LAR power plant is farthest away from the existing database.

It must be pointed out that experimental databases on the RS and LAR concepts are not as developed as for the other tokamak concepts. For the reversed shear mode of operation, significant advances in plasma performance were reported recently on TFTR [38] and on DIII-D [39]. Both experiments reported significant enhancements in energy confinement for both electrons and ions inside the RS region, leading to a highly peaked pressure profile near the axis. Of special interest are the DIII-D results which indicate transitions from the L-mode to the ELMy or ELM-free H-mode for these discharges with central reversed shear. This leaves open the possibility that the H-mode data presented in Figs. 5.2-6 and 5.2-7 may indeed be relevant to the RS mode. As for the LAR concept, the most advanced results have been from the START spherical tokamak [40], where the measured τ_E is typically twice the neo-Alcator value, and is well represented by the

Rebut-Lallia scaling. Data from double-null-divertor discharges on this machine appear to indicate transition to an improved confinement regime at high currents and densities. However, there is no data on auxiliary heated discharges. Data on larger LAR experiments with higher currents, external heating power and current drive must be developed before this mode of operation can be used in a power plant.

5.2.4. Heat Exhaust

In a fusion power plant, the core plasma is continuously heated by several hundred megawatts of α power, P_α and by the non-inductive current power, P_{CD}. The need to remove the charged-particle heat escaping the tokamak plasma in a timely fashion is an issue of critical importance in designing a fusion power plant. This power crosses the separatrix into the scrape-off layer and is deposited on the divertor plates. The average heat flux striking the divertor plate is approximated by

$$q_{PLATE} = \frac{1}{2\pi\lambda_{div}} \frac{P_{PLATE}}{R}, \tag{5.2-10}$$

where λ_{div} is the expanded power scale length measured along the divertor plate, R is the major radius, and P_{PLATE} is the net power reaching the divertor plate. As a point of reference, the engineering design goal for fusion power plants is to limit the peak heat flux at the plates to $\sim$5 MW/m^2.

Denoting P_{tr} as the power that crosses the separatrix and f_{rad} as the fraction of total plasma heating power, $P_\alpha + P_{CD}$, that is radiated in the plasma core and the edge radiative mantle, then

$$P_{tr} = (P_\alpha + P_{CD})[1 - f_{rad}]. \tag{5.2-11}$$

If there is no radiation in the scrape-off layer and the divertor region, then $P_{plate} = P_{tr}$. In this case, f_{rad} values of about 0.8 to 0.9 is necessary for a tokamak power plant in order to satisfy the above engineering design goal. This value of f_{rad} can be achieved by introducing impurities in the plasma edge creating a radiative edge mantel. However, the presence of these impurities can increase the current-drive power substantially. Another way to reduce the peak heat flux is to introduce impurities into the divertor region and allow for friction forces to entrain the impurities in the divertor region without increasing the Z_{eff} of the core plasma dramatically.

The atomic physics processes of potential importance in the plasma and divertor chamber include bremsstrahlung and impurity line radiation, and charge exchange. Since

the excitation energies of these processes are fixed constants, the ratios between the reference plasma temperature and these values are determined by the absolute magnitude of the former. Lackner [26] has extended this observation to demonstrate that under the condition of constant (or known) plasma temperature, similarity laws are obeyed in the plasma edge with the result that the quantity P_{tr}/R is in fact equivalent to the dimensionless figure-of-merit that characterizes the regime of divertor operation. This figure of merit has also been independently derived [27] by using the scaling transformation properties of the system of two dimensional fluid plasma and neutral equations together with boundary conditions [28].

We therefore can use the quantities P_{tr}/R and f_{rad} as figures of merit for comparing the divertor heat removal requirements in a given power plant candidate to the existing experimental database. It is essential that reactor-level values of both of these parameters be obtained simultaneously in order to demonstrate feasibility. An important caveat is that this must be achieved without a significant buildup of the injected impurity in the core. This is characterized by the requirement that $Z_{eff} < 2.6$ for low-Z impurities. Attainment of these parameters will likely involve a splitting of the radiating power between the plasma center, mantle, scrape-off layer, and divertor, and will also likely require density compression of the impurity species in the divertor region.

Data points for heat removal in several tokamak experiments are given in Fig. 5.2-8. In cases where there is no impurity injection [29], values of f_{rad} in the range of 0.4–0.6 is obtained by intrinsic carbon radiation in detached plasmas, *e.g.,* on TEXTOR, C-Mod, ASDEX-U, JET, JT-60U and DIII-D. For discharges with neon puffing, such as in TEXTOR, ASDEX-U, and DIII-D, a total radiation fraction in the range of 0.9 is obtained. In the case of TEXTOR [30], where a pumped limiter was used, a radiating mantle was set up with a resultant $f_{rad} = 0.95$. Completely detached ELM-free H-mode experiments on ASDEX-U [31] show that f_{rad} can reach as high as 0.9 through a combination of D and Ne puffing, whereas f_{rad} drops to 0.55 without Ne puffing. In DIII-D [32], Ne puffing resulted in the simultaneous creation of a radiative mantle and a strong radiation zone near the divertor plates, with each region radiating approximately equal power.

In Fig. 5.2-8 the range of design values of f_{rad} and P_{tr}/R for the five Starlite power plant options are also plotted. It is clear from this figure that the experimental database has already reached the desired value of f_{rad} for power plants, either by the action of a radiative mantle, or a combination of both scrape-off layer and core radiation. However, these data points have been achieved at levels of P_{tr}/R that are still some distance away from those in power plants.

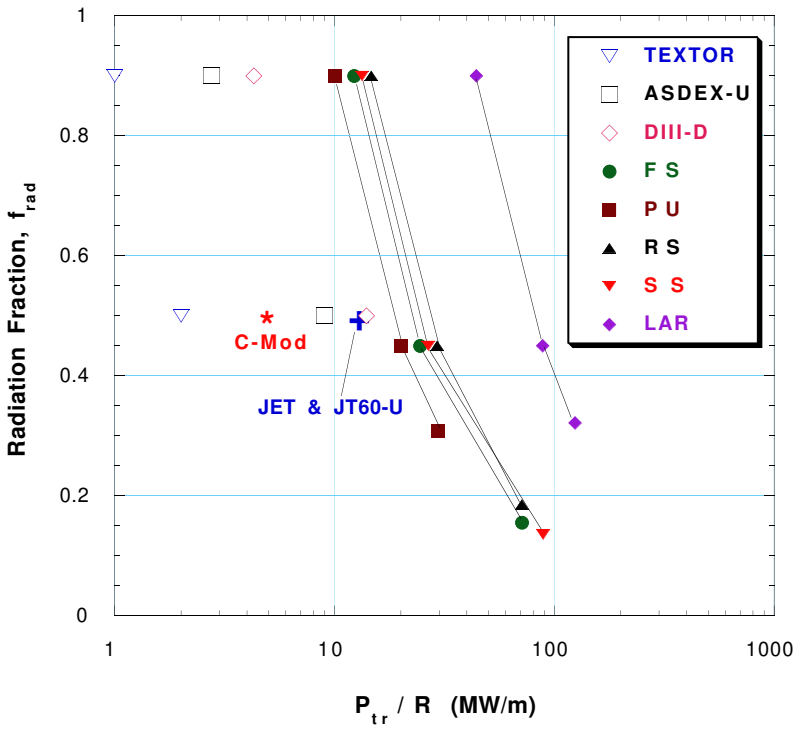

Figure 5.2-8. Plot of heat exhaust figures of merit, f_{rad} versus P_{tr}/R, for a number of present experiments (TEXTOR, C-Mod, JET, JT60-U, ASDEX-U, and DIII-D), and design values for the five Starlite fusion power plant options (FS, PU, RS, SS, and LAR). The dotted and chain-dotted lines represent the trend of PU option and LAR respectively due to the variation of f_{rad}. Options FS, RS, and SS follow the chained line. Note that f_{rad} of PU fusion power plant is relatively high compared to the other concepts because no current-drive power is required.

If the peak solid target heat flux is to be limited to values $\sim$5 MW/m^2, a combination of enhanced radiation in the core, in the scrape-off layer, and in the divertor is required. The feasibility of obtaining this has not yet been demonstrated, but it may be possible using techniques such as impurity density compression in the divertor region.

5.2.5. Helium Ash Removal

Effective removal of the helium ash produced by the fusion reactions is an important issue for fusion plasma [41–43]. It becomes increasingly difficult to maintain an ignited plasma the greater the helium concentration. This is due to dilution of the fuel ions with helium which reduces the fusion yield, the enhanced radiation losses associated with the

higher Z helium. It is well known that with helium present the energy confinement time must increase to compensate for the above effects. To examine the impact of helium ash accumulation in a fusion power plant, one can use a simple power balance for the core plasma in steady state, by neglecting radiation and current drive power, ignoring any impurities other than helium, and by considering all plasma species to have the same temperature and energy confinement time. At fixed β, the ratio of energy confinement times with and without the presence of helium can be written as

$$\frac{\tau_E^{wHe}}{\tau_E^{w/oHe}} = \left(1 + \frac{3}{2}\frac{n_{He}}{n_i}\right)^2 . \tag{5.2-12}$$

Clearly the presence of helium in the core plasma requires an increased energy confinement time to maintain power balance.

From steady-state helium particle balance in the core plasma (ignoring other impurities), the ratio of helium to the fuel ion density is given by

$$\frac{n_{He}}{n_i} = \frac{\tau_{He}}{(1 - R_{He})}\frac{n_i\langle\sigma v\rangle}{4} = \tau^*_{He}\frac{n_i\langle\sigma v\rangle}{4} , \tag{5.2-13}$$

where n_i is the D–T fuel ion density, n_{He} is the helium density, $\langle\sigma v\rangle$ is the fusion reaction rate, R_{He} is the helium recycling coefficient, and τ_{He} is the helium particle confinement time in the core plasma. The ratio of the core plasma helium confinement time to $(1 - R_{He})$ is referred to as the effective confinement time τ^*_{He}. This time constant has physical significance in that it reflects the mean residence time of a helium particle before finally being pumped out of the plasma chamber.

Since many transport theories relate the particle confinement time to the energy confinement time, the ratio of τ^*_{He}/τ_E is often used to measure the effectiveness of core ash removal. From the simple power balance above (ignoring bremsstrahlung radiation and current-drive power) and helium particle balance, one can derive

$$\frac{\tau^*_{He}}{\tau_E} = \frac{\frac{n_{He}}{n_i}}{\left(1 + \frac{3}{2}\frac{n_{He}}{n_i}\right)}\left(\frac{E_\alpha}{3kT}\right) , \tag{5.2-14}$$

where E_α is the alpha birth energy (3.5 MeV). Equation 5.2-14 shows that as τ^*_{He} increases, the helium fraction in the plasma core increases. However, as pointed out earlier, τ_E must then increase in order to maintain the operating point. This ratio is therefore the condition required on τ^*_{He} in order to achieve power balance in a D–T fusion plasma with a given helium to fuel ion density ratio.

Including both bremsstrahlung radiation and a single impurity with charge Z, the ratio of helium particle confinement time to energy confinement time is given by,

$$\frac{\tau_{He}^*}{\tau_E} = \frac{\frac{n_{He}}{n_i}}{\left(1+\frac{3}{2}\frac{n_{He}}{n_i}+\frac{Z+1}{2}\frac{n_Z}{n_i}\right)}\left(\frac{E_\alpha}{3kT}\right)\left[1-\frac{4C_{br}T^{0.5}}{\langle\sigma v\rangle E_\alpha}Z_{eff}\left(1+\frac{2n_{He}}{n_i}+\frac{Zn_Z}{n_i}\right)^2\right] \quad (5.2\text{-}15)$$

where C_{br} is the prefactor in the standard global expression for bremsstrahlung power, and the plasma temperature is taken as the volume average. The ratio $4C_{br}T^{0.5}/\langle\sigma v\rangle E_\alpha$ is about 0.1 for a 10-keV plasma. Comparing Eqs. 5.2-14 and 5.2-15 shows that the introduction of impurities and radiation leads to a lower value of τ_{He}^*/τ_E to maintain a fixed ratio of helium to fuel ions in the plasma, and is a more restrictive condition. As an example, a plot of τ_{He}^*/τ_E is given in Fig. 5.2-9 for various helium to fuel ion ratios as a function of the volume average plasma temperature, and assuming a 1% oxygen impurity level. According to this simple calculation, for an average temperature of 10 keV, the ratio τ_{He}^*/τ_E increases from 4 to 12 as n_{He}/n_i is varied from 0.05 to 0.3. For the same helium concentration, it is interesting to point out that there is an optimum temperature at which the requirement on τ_{He}^*/τ_E is most relaxed, *i.e.,* when the ratio is a maximum.

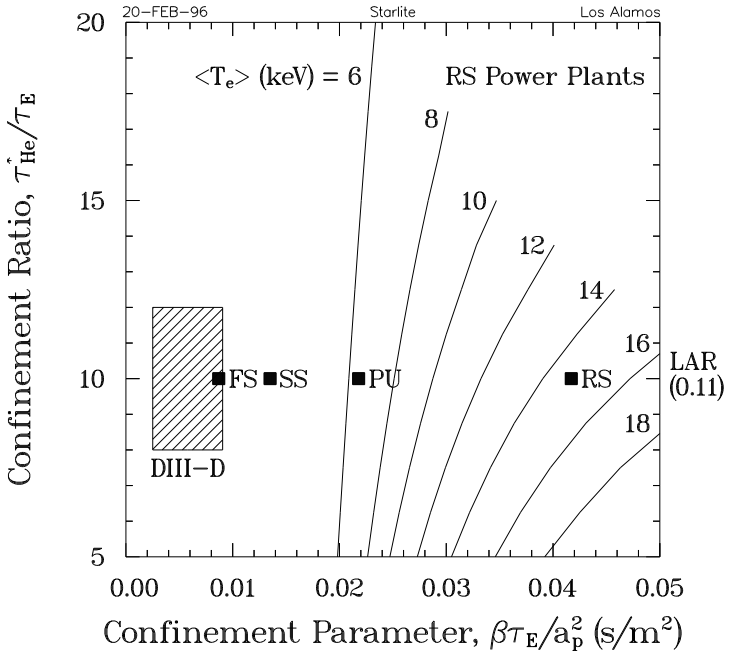

Figure 5.2-9. Ratio of effective ash confinement to energy confinement time required for power balance as the averaged plasma temperature and the ratio of ash to fuel ion densities are varied. An oxygen impurity concentration of 1% is assumed.

A figure of merit for helium ash removal should reflect the critical requirements of a fusion power plant and provide a basis for experimental tokamaks to gauge their progress toward these requirements. The primary issues for helium ash removal are:

1. sufficiently short effective ash particle confinement time; τ^*_{He}
2. low non-helium impurity content; and
3. reasonable pumping speed and fueling requirements.

The difficulty with constructing a figure of merit for helium ash removal lies with the fact that the negative impact of helium in the core plasma is not properly represented without an ignited plasma. The fusion power plant requirement for τ^*_{He}/τ_E is determined by two constraints, helium particle balance and ignited plasma power balance. For a given amount of helium in the plasma there is a corresponding particle confinement time and energy confinement time. In present day experiments, the plasma energy confinement time is unaffected by the presence of the helium. Therefore care must be taken when drawing a direct correlation between the τ^*_{He}/τ_E from an experiment to a power plant. The question arises whether the original energy confinement time in the experiment, properly scaled to the power plant parameters, would be sufficient to maintain ignition with the given helium fraction in the plasma.

With this difficulty in mind, it is recommended that that ratio τ^*_{He}/τ_E be presented simultaneously with the value of $\beta\tau_E/a_p^2$, which measures the energy confinement performance of the plasma (see Sec. 5.2.3). Knowing the range of $\beta\tau_E/a_p^2$ values required for ignited plasma power balance would help to indicate how well experiments are actually simulating the power plant situation.

The problem caused by non-helium impurities is the displacement of fuel ions by the impurity ions and their associated electrons. A reasonable measure for this is simply Z_{eff}, and this should be minimized as much as possible.

The pumping and fueling figure of merit should represent the desire to remove helium particles efficiently and not remove fuel particles. A parameter developed in power plant studies to reflect this is called the burn-up fraction, and is given by

$$f_b \;=\; \frac{2\Gamma_{He}}{2\Gamma_{He}+\Gamma_i} \tag{5.2-16}$$

and would take on the value of unity if only helium and no fuel were removed. Here, Γ_{He} and Γ_i are the flux of He and D–T-fuel ions that are removed from the plasma.

The general scheme for removing the helium ash is to use a pumped divertor, where some fraction of the helium leaving the plasma core is pumped out of the chamber. In this case, $\Gamma_{He} = n^p_{He} S^{eff}_{He}$ and $\Gamma_i = n^p_i S^{eff}_i$, where S^{eff} is the effective pumping speed (m^3/s), n^p is the neutral particle density at the pump aperture.

The balance for helium and fuel pumping can be approximately treated separately, so that the burn-up fraction can be related to quantities measurable in an experiment, as in

$$f_b = \frac{2\frac{n_{He}}{\tau^*_{He}}}{2\frac{n_{He}}{\tau^*_{He}} + \frac{n_i}{\tau^*_i}} . \tag{5.2-17}$$

Using Eq. 5.2-13 the above expression can be shown to be equivalent to the standard definition of the burn-up fraction,

$$f_b = \frac{1}{1 + \frac{2}{n_i \tau^*_i \langle \sigma v \rangle}} . \tag{5.2-18}$$

Since this quantity is also known for power plant designs, comparisons can be made directly with experiments, to ensure that the experimental system is providing a scaled model of the reactor system.

Significant strides have been made recently in developing the database on active particle removal experiments, notably on TEXTOR and DIII-D. The first substantial work on pumped discharges comes from TEXTOR [44,45]. This device has eight separate limiters around the torus and each is equipped with a turbomolecular pump. Active pumping of the helium gas was clearly demonstrated, and the measured τ^*_{He}/τ_E values are in the range of 10–30 in L-mode discharges. The helium particle confinement time in the core has been calculated, with τ_{He}/τ_E reported to be in the range 1–2. In ELM-free H-mode discharges, values of τ^*_{He}/τ_E of about 70 were observed. Also for these experiments, the exhaust efficiency $(1 - R_{He})$ was found to increase with increasing plasma density.

A series of experiments on helium removal have been performed on DIII-D. First, experiments with no helium pumping [45] clearly showed that the presence of ELMs enhanced the efflux of helium from the plasma edge. More recent data on DIII-D [46], using the argon frosted cryopump for pumping helium that is gas puffed into the plasma chamber, indicates a τ^*_{He}/τ_E value of approximately 8, in ELMy H-modes. It was later shown that, with central helium fueling from a neutral beam, τ^*_{He}/τ_E of about 11 was achievable. These experiments indicate that control of helium in the plasma may be achieved even in H-mode discharges, so long as ELMs are present, and represent the

most power plant relevant results to date. In addition, helium transport studies [47] found that the helium and electron density profiles were nearly identical, indicating that helium accumulation is not taking place. This was shown to be the case for L-mode, H-mode, ELMy H-mode, and VH-mode confinement regimes.

The range of measured values for the helium-removal figure of merit on DIII-D are shown in Fig. 5.2-9, as a function of $\beta\tau_E/a_p^2$. Also shown are the contours for ignited power balance, where a power plant can operate, at various volume-average temperatures. These results correspond to a reversed shear configuration with $A = 4.0$, $R = 5.6$ m, and $B_T = 7$ T. They include profile effects, and indicate that one needs to achieve low τ^*_{He}/τ_E and high $\beta\tau_E/a_p^2$ simultaneously for fusion power-plant operation. Also displayed in Fig. 5.2-9 are the five Starlite power-plant candidates, for which $\tau^*_{He}/\tau_E = 10$ has been assumed, resulting in required $\beta\tau_E/a_p^2$ values ranging from 0.0078 for FS to 0.11 for LAR options.

5.3. CONCEPT EVALUATION

The five tokamak operating modes that have been evaluated by the Starlite project are: (1) a steady state, first stability regime (FS) similar to ARIES-I [1]; (2) a pulsed, first stability regime (PU) similar to PULSAR [2]; (3) a steady state, second stability (SS) regime similar to ARIES-II/IV [3]; (4) a steady state, reversed shear (RS) mode [4]; and (5) a steady state, low aspect ratio configuration [5]. Operating parameters for the five Starlite tokamak power plant concepts under consideration are listed in Table 5.3-I and described in the following subsections.

5.3.1. First Stability [ARIES-I]

The first-stability tokamak power plant concept (FS) is a modification of the ARIES-I [1] design, but with the peak toroidal field at the coil lowered from the ARIES-I value of 21 T to a more practical value of 16 T. Additionally, the SiC-composite blanket and shield have been replaced with the same vanadium blanket and shield as the other power plant candidates, for purposes of a common-base comparison. The normalized beta value is $\beta_N = 2.88$, which we calculate to be 10% below the beta limit that is self-consistent with the design pressure and current profiles. The values of $q_0 = 1.3$ and $q_* = 3.77$ were determined by a tradeoff between high β (and low q) and high bootstrap fraction (and high q). The design utilized relatively modest shaping parameters of $\kappa_X = 1.8$ and $\delta_X = 0.7$

Table 5.3-I.
Parameters for the Five Starlite Power Plant Candidates

	FS	PU	RS	SS[(a)]	LAR
Plasma aspect ratio, $A = R/a_p$	4.0	4.0	4.0	4.0	1.25
Major radius, R(m)	7.96	8.68	5.04	6.40	5.00
Plasma minor radius, a_p(m)	1.99	2.17	1.26	1.60	4.00
Plasma elongation, κ_X	1.81	1.80	1.99	2.03	3.40
Plasma triangularity δ_X	0.71	0.50	0.69	0.67	0.55
Cylindrical safety factor q_*	3.77	2.40	2.37	4.60	3.54
Central Safety factor, q_0	1.3	0.7	2.8	2.0	2.9
Stability parameter, $\epsilon\beta_p$	0.54	0.32	0.56	1.22	1.14
Normalized beta, $\beta_N(\%)$	2.88	2.70	4.76	5.28	6.42
Beta parameter, $\beta/\epsilon(\%)$	8.12	10.00	21.24	12.17	45.36
Confinement ratio, τ^*_{He}/τ_E	10.0	10.0	10.0	10.0	10.0
Ignition parameter, $\beta\tau_E/a_p^2(\%\mathrm{s/m}^2)$	0.78	2.18	4.17	1.35	11.05
ITER-89P scaling multiplier, H	1.71	2.38	2.40	2.47	3.02
Normalized confinement multiplier, H/q_*	0.45	0.99	1.01	0.54	0.85
Plasma current, I_p(MA)	12.6	15.0	10.3	7.72	40.1
Bootstrap-current fraction, f_{BS}	0.57	0.34	0.89	>1	0.997[(b)]
Current-drive efficiency, $\gamma_B(10^{20}\mathrm{A/Wm}^2)$	0.56	NA	2.02	0.49	34.2
Current-drive power to plasma (MW)	236.6	0	64.7	199.1	7.3
On-axis toroidal field, B_T(T)	8.99	7.46	7.35	8.37	1.77
Peak field at TF coil, B_{TF}(T)	16.0	13.1	15.7	15.9	14.8
Normalized heat flux, P_{tr}/R(MW/m)	71.2	29.5	71.3	89.0	124.2
Recirculating power fraction, $(1/Q_E)$	0.29	0.06	0.13	0.33	0.63
COE (mill/kWh)	99.7	130.2	69.7	92.6	116.0

(a) This design is not optimized to the lowest COE.

(b) Includes diamagnetic current.

that allowed passive stabilization of a double-null plasma with the stabilizer behind the breeding blankets, and at the same time minimized the PF coil energy. A combination of ICRF fast wave and lower hybrid wave was used as the current drive system. The total current drive power required is high (237 MW) because of the relatively low bootstrap fraction of 0.57. The ignition parameter of $\beta\tau_E/a_p^2 = 0.79$ and the value of $H/q_* = 0.45$ are the most modest of all the design concepts.

5.3.2. Pulsed Operation [PULSAR]

The pulsed-tokamak power plant concept (PU) is a modification of the PULSAR [2] design, with a reduced normalized beta value of $\beta_N = 2.70$, which we calculate to be 10% below the beta limit. The design also uses the common vanadium blanket and shield design described in Sec. 6. that represents a refinement over the original PULSAR blanket and shield. The current profile is calculated self-consistently from the requirement that the plasma be in an ohmic stationary state with no external current drive, and that the bootstrap current and plasma resistivity be consistent with the pressure and the temperature profiles. The design utilized the same modest shaping of $\kappa_X = 1.8$ and $\delta_X = 0.5$ as did the FS design. The ignition parameter of $\beta\tau_E/a_p^2 = 2.18$ and the value of $H/q_* = 0.99$ are significantly larger than those required for the FS design. The recirculating power fraction is very low since the design uses only ohmic current drive which has very high efficiency. The fact that the tokamak is pulsed causes the design value of the peak field at the coil to be 18% lower than for steady state designs (FS), and the fact that there is no control over the current profile causes the β_N to be 6% lower.

5.3.3. Second Stability [ARIES-II/IV]

The second stability tokamak power plant concept (SS) is an updated version of the ARIES-II [3] design, where a more accurate bootstrap current model [49] with full α pressure representation has been applied. As with the other options, the pressure is lowered to give a 10% margin against the MHD stability limit, and a refined vanadium blanket and shield design has been used. five power plant options. The design has a normalized beta value of $\beta_N = 5.28$ (wall stabilized), but with very large central and cylindrical safety-factor values of $q_0 = 2.0$ and $q_* = 4.6$ in order to obtain the high values of $\epsilon\beta_p$ needed for full second stability access. This design, which is not optimized with respect to the COE, has a value of $\beta/\epsilon = 12$, only about 50% higher than FS. But the bootstrap-current fraction, f_{BS}, exceeds unity, with the equilibrium

having a substantial bootstrap overdrive in the bulk plasma, and a plasma current of $I_p = 7.72$ MA, significantly enhancing the recirculating power over that of ARIES-II. The ignition parameter of $\beta\tau_E/a_p^2 = 1.35$ and the value of $H/q_* = 0.54$ are larger than for the FS design, but still within the existing tokamak data base. The design uses a combination of ICRF fast-wave current drive to provide the seed current on axis and lower-hybrid current drive to offset the overdriven bootstrap current in the bulk plasma region and to tailor the current profile near the edge.

5.3.4. Reversed Shear

The reversed shear tokamak power plant concept (RS) grew out of analysis performed for the TPX program [4]. Its combination of a current profile peaked off axis and a peaked pressure profile leads to a self-consistent design with a normalized beta value of $\beta_N = 4.76$ (wall stabilized), and to a value of $\beta/\epsilon = 21.2$, over twice as large as FS, but also to a value of the bootstrap-current fraction of $f_{BS} = 0.89$, leading to a very low recirculating power fraction. The ignition parameter of $\beta\tau_E/a_p^2 = 4.17$ and the value of $H/q_* = 1.01$ are larger than for the FS design, but probably justified in light of the recent experimental results [38, 39] showing greatly reduced transport in the reversed shear configuration.

5.3.5. Low-Aspect-Ratio

The low-aspect-ratio tokamak [5] (LAR) differs from the others in that the TF coils are made of normal-conducting copper rather than superconducting, and that there are no OH coils on the inboard side. Little or no shielding is provided on the inboard side of the tokamak in order to attain very low aspect ratios. Detailed MHD stability calculations show that it is possible to find stable equilibria at very low aspect ratios with high values of the normalized beta which simultaneously allows for high beta and high bootstrap fraction. The reference LAR design has an aspect ratio of $A = 1.25$, a normalized beta value of $\beta_N = 6.42$ (wall stabilized), and a value of $\beta/\epsilon = 45.4$, significantly larger than the other designs. The bootstrap current density profile is well aligned with the equilibrium current profile over most of the plasma cross section, so that the pressure-driven current (bootstrap+diamagnetic) is calculated to be 99.7% of the plasma current, the seed current being located near the magnetic axis. As a result, the current-drive power requirement of 7.3 MW (low-frequency fast wave) is the lowest among the steady state candidates. One caveat of this result could be that the current-drive power is extremely

sensitive to variations in the plasma profiles. The ignition parameter of $\beta\tau_E/a_p^2 = 11.1$ and the value of $\gamma_B = 34.2$ are largest of the five concepts but since there is so little data available for the Low-A configuration, it is impossible to determine how credible this is. The large amount of power dissipated by the copper coils leads to a very large recirculating power fraction.

5.4. Starlite Reference Design

Five Starlite power plant designs based on five distinct operating modes have been analyzed by the systems code, using a common basis of economics and engineering assumptions. The results of these analyses in terms of the design physics FOM and COE values for the five candidates have been presented in Table 5.3-I for comparison. The ARIES systems code is used to estimate the cost of electricity (COE) values for these options using the same economic assumptions [48]. The blanket and shield design used for all five power plant candidates is a refinement of the ARIES-II vanadium blanket and shield, and is described in Sec. 6.

Except for the second stability (SS) option, each of the concepts corresponds to a self-consistent power plant design (at the level of systems code) optimized to its unique set of design choices. While the absolute values for the COE reflect a high degree of uncertainty in material costs and the fact that each design is not completely optimized through a rigorous design study, we believe that the relative rankings of the five concepts are accurate given present understanding and data base.

The first-stability options, steady0state (FS) and pulsed-plasma (PU) require relatively modest extrapolations in physics parameters from the present database. The pulsed-plasma tokamak is the most expensive and appear to be unattractive as a power plant. The COE for the FS design is higher than the requirements established for the Starlite designs (Sec. 2). Most probably this design requires the use of high-field magnets and advanced SiC-composite blankets (to achieve a high level of safety) to become attractive.

The low-aspect ratio tokamak is furthest from the experimental data base, practically in all the critical physics areas. (However, this is somewhat mitigated by the recent theoretical analysis that shows that its operating point may in fact be achievable.) It is also the second least economical (after PU) of the five concepts with a COE value of 116 mills/kWh. These findings, together with the rather modest parameter ranges for present and planned LAR experiments [40], and a number of high-leverage but yet

unresolved engineering issues (see Sec. 8), precludes the LAR concept from our present consideration for the reference Starlite power plant. Nevertheless, this design is the least developed of Starlite candidates and the power plant potential of the LAR concept is sufficiently high as to warrant further investigation and, perhaps, a future full-scale evaluation.

Of the remaining candidates, the reversed-shear concept is the most attractive in terms of economics, having a COE of ∼70 mills/kWh, that is significantly lower than those of the rest. The second-stability option is second in terms of economics. There is reason to believe that the second-stability equilibrium could be better optimized to better align the bootstrap current with the equilibrium current, and thus further minimize the required external current drive. However, even so, it is believed that the projected COE values for the SS power plant will not fall below 80–90 mills/kWh. Also there is theoretical concern that the second-stability configuration may be difficult to maintain in practice, since a lowering of the pressure gradient locally would cause an instability region to develop and propagate, thus making it configurationally unstable. Lastly, the is not experimental data for this concept.

Overall, the Starlite team concluded that the reversed-shear plasma offer the combination of sound economic potential and a growing experimental data base as many key aspects of the reversed-shear concept have already been demonstrated in several devices (*e.g.,* TFTR, DIII-D, JET, and Tore Supra).

5.5. SUMMARY AND CONCLUSIONS

Physics performance assessments have been carried out, in conjunction with systems analyses, in order to select the best realizable and economically attractive fusion power plant design among five different options. These candidates include tokamak operating modes similar to ARIES-I, ARIES-II/IV, PULSAR, the reversed shear mode, and the low-aspect-ratio magnetic configuration, and are labeled FS, SS, PU, RS and LAR, respectively.

To facilitate the physics analysis, plasma performance parameters, or figures of merit (FOM), in five critical physics areas have been identified with the intent to keep track of progress in achieving the required performance levels for the power plant. The five physics areas of interest are MHD stability, current drive, heat exhaust, energy confinement and helium ash removal. To be inclusive of the five operating mode candidates, attempt has been made to select the FOMs based on fundamental performance quantities that

are measurable in experiments and that are independent of plasma size and machine parameters. The identified figures of merit are given as follows:

- **MHD Stability:**
  - Power density parameter: β/ϵ
  - Stability parameter: $\epsilon\beta_p$
- **Current Drive:**
  - Normalized current-drive efficiency: $\gamma_B \equiv \overline{n}_e I_p R/P_{CD}$
- **Energy Confinement:**
  - Ignition parameter: $\beta\tau_E/a_p^2$
  - Power density parameter: β/ϵ
- **Heat Exhaust:**
  - Normalized heat flux: P_{tr}/R
  - Total radiation fraction: f_{rad}
- **Helium ash removal:**
  - Particle confinement parameter: τ_{He}^*/τ_E
  - Ignition parameter: $\beta\tau_E/a_p^2$
  - Effective charge: Z_{eff}
  - Helium burn-up fraction: f_b

In Sec. 5.2 values for these figures of merit in the five critical physics areas that were measured in experiments are plotted along with the design values for the five Starlite power plant options. Based on the results displayed in these figures, it is clear that the FS and PU power plant options have physics performance parameters that are closest to the existing database. On the other hand, the LAR concept demands the largest physics performance extrapolations from the most recent data obtained in machines operating in this mode. Taking into account the projected COEs for the five power plant options as given in Table 5.3-I, we conclude that the RS and SS modes of operation are the most attractive among the candidates, because they have the lowest COEs. Among these two options, the reversed shear concept presently emerges as the best choice for the reference

power plant design. This is because it is economically superior, is significantly closer to having been experimentally prototyped in each of the key tokamak physics areas than the second stability concept, and therefore has the least uncertainty in achieving the required values of all of the physics parameters at a reasonable cost.

Having chosen the reversed-shear concept as the basis for the Starlite reference power plant design, it is useful to identify physics areas in which to focus present and future research efforts towards realizing this goal. We first note that the experimental data that are used in this study are taken entirely from L-mode and H-mode discharges, without the use of any profile tailoring. Thus, a systematic development and collection of database for reversed shear discharges on large high-power devices are in order, including all five aforementioned critical physics areas. From a broader perspective, it is also clear that the existing tokamak database does not contain discharges that simultaneously achieve values of all the physics FOM parameters needed to make an attractive fusion power plant. This highlights the need for continued physics research aimed at concept improvement, in particular in developing modes of tokamak operation that prototype power plant values of each of the FOMs identified. Finally, we emphasize the need to develop experimental database in long pulse or steady state discharges with the use of current drive and profile control in fusion relevant regimes.

REFERENCES

[1] F. Najmabadi, R. W. Conn, *et al.*, "The ARIES-I Tokamak Fusion Reactor Study—The Final Report," UCLA report UCLA-PPG-1323 (1991); also, R. W. Conn, F. Najmabadi, *et al.*, "ARIES-I: A Steady-State, First-Stability Tokamak Reactor with Enhanced Safety and Environmental Features," *Proc. 13th Int. Conf. on Plasma Phys. and Controlled Nucl. Fusion Research,* Washington, D.C. (Oct. 1990), International Atomic Energy Agency, Vienna (1991) 659.

[2] F. Najmabadi and the ARIES Team, "The PULSAR Pulsed-Tokamak Power Plant Study," University of California San Diego report (to be published).

[3] F. Najmabadi, R. W. Conn, *et al.*, "The ARIES-II and -IV Second-Stability Tokamak Fusion Power Plant Study—The Final Report," UCLA report UCLA-PPG-1461 (to be published); also, F. Najmabadi, R. W. Conn, *et al.*, "Directions for Attractive Tokamak Reactors: The ARIES-II and ARIES-IV Second-Stability Designs," *Proc. 14th Int. Conf. on Plasma Phys. and Controlled Nucl. Fusion Research,* Würzburg, Germany (Oct. 1992), International Atomic Energy Agency, Vienna (1993) 295.

[4] C. E. Kessel, J. Manickam, G. Rewoldt, W. M. Tang, "Improved Plasma Performance in Tokamaks with Negative Magnetic Shear," *Phys. Rev. Lett.* **72** (1994) 1212.

[5] Y-K. M. Peng, "Prospects and Status of Low-Aspect-Ratio Tokamaks," *Trans. Fusion Technol.* **27** (1995) 138.

[6] T. K. Mau, D. A. Ehst, S. C. Jardin, C. E. Kessel, B. J. Lee, "Plasma System Requirements and Performance Data Base for the Starlite/Demo Fusion Power Plant," *Proc. IEEE 16th Symp. on Fusion Eng.,* Champaign, IL (Oct. 1995) IEEE No. 95CH35852, IEEE, Piscataway, NJ (1995) 1194.

[7] H. R. Strauss, "Dynamics of High β Tokamaks," *Phys. Fluids* **20** (1977) 1354.

[8] N. Pomphrey, "Bootstrap Dependence on Plasma Profile Parameters," Princeton Plasma Physics Laboratory report PPPL-2854 (1992).

[9] P. A. Politzer, T. Casper, C. B. Forest, *et al.,* "Evolution of High β_p Plasmas with Improved Stability and Confinement," *Phys. Plasmas* **1** (1994) 1545.

[10] J. Menard, S. C. Jardin, S. M. Kaye, *et al.,* "Ideal MHD Stability of High Beta/High Bootstrap Fraction Equilibria in NSTX," *Bull. Am. Phys. Soc.* **40** (1995) 1655.

[11] J. J. Ramos, "Theory of the Tokamak Beta Limit and Implications for Second Stability," *Phys. Fluids B* **3** (1991) 2247.

[12] M. S. Chance, S. C. Jardin, T. Stix, "Ballooning Mode Stability of Bean-Shaped Cross Sections for High-β Tokamak Plasmas," *Phys. Rev. Lett.* **51** (1983) 1963.

[13] A. Bondeson and D. J. Ward, "Stabilizaton of External Modes in Tokamaks by Resistive Walls and Plasma Rotation," *Phys. Rev. Lett.* **72** (1994) 2709.

[14] D. A. Ehst, S. C. Jardin, and C. E. Kessel, "Starlite Figures of Merit for Tokamak Current Drive–Economic Analysis of Pulsed and Steady State Power Plants with Various Engineering and Physics Performance Parameters," Argonne National Laboratory report ANL/FPP/TM-284 (1995); also *Proc. IEEE 16th Symp. on Fusion Eng.,* Champaign, IL (Oct. 1995) IEEE No. 95CH35852, IEEE, Piscataway, NJ (1995) 1182.

[15] N. J. Fisch, "Theory of Current Drive in Plasmas," *Rev. Mod. Phys.* **59** (1987) 175.

[16] D. A. Ehst, K. Evans, Jr., "Multiple Wave Radiofrequency Current Driven Tokamak Reactors in the First Stability Regime," *Nucl. Fusion* **27** (1987) 1267.

[17] D. A. Ehst, C. F. F. Karney, "Approximate Formula for Radiofrequency Current Drive Efficiency with Magnetic Trapping," *Nucl. Fusion* **31** (1991) 1933.

[18] D. A. Ehst, K. Evans, Jr., D. W. Ignat, "Tokamak MHD Equilibrium Generation by Narrow-spectrum Fast-Wave Current Drive," *Nucl. Fusion* **26** (1986) 461.

[19] J. D. Lee, Tech. Editor, "TIBER II/ETR Final Design Report," Vol. **1** (1987).

[20] T. Imai, H. Kimura, Y. Kusama, *et al.,* "Lower Hybrid Current Drive and Higher Harmonic ICRF Heating Experiments on JT-60," *Proc. 13th Int. Conf. on Plasma Phys. and Controlled Nucl. Fusion Research,* Washington, D.C. (Oct. 1990), International Atomic Energy Agency, Vienna (1991) 645.

[21] J. S. deGrassie, C. C. Petty, R. I. Pinsker, *et al.,* "Fast Wave Current Drive on DIII-D," *Proc. 11th Top. Conf. on Radio Frequency Power in Plasmas,* Palm Springs, CA (1995) 173. Data point at $T_{e0} = 6.3\,\mathrm{keV}$ is unpublished and provided by C. C. Petty.

[22] X. Litaudon for Equipe Tore Supra, "RF Heating and Current Drive in Tore Supra," in 11th Top. Conf. on *Radio Frequency Power in Plasmas,* Palm Springs, CA (1995). Data point from R. Goldston.

[23] J. H. Rogers, PPPL, private communication (1995).

[24] C. Gormezano for the JET Team, "Non-Inductive Current Drive in JET," *Proc. 14th Int. Conf. on Plasma Phys. and Controlled Nucl. Fusion Research,* Würzburg, Germany (Oct. 1992), International Atomic Energy Agency, Vienna (1993) 587.

[25] S. Itoh, N. Hiraki, Y. Nakamura, *et al.,* "Experiments on Steady-State Tokamak Discharge by LHCD in TRIAM-1M," *Proc. 13th Int. Conf. on Plasma Phys. and Controlled Nucl. Fusion Research,* Washington, D.C. (Oct. 1990), International Atomic Energy Agency, Vienna (1991) 733.

[26] K. Lackner, "Figures of Merit for Divertor Similarity," *Comments Plasma Phys. Contr. Fusion* **15** (1994) 359.

[27] P. J. Catto, S. Krasheninnikov, and J. W. Conner, "Scaling Laws for Two-Dimensional Divertor Modeling", Massachusset Institute of Technology report PFC/JA-95-10 (1995).

[28] P. J. Catto, "A Short Mean-Free Path, Coupled Neutral-Ion Transport Description of a Tokamak Edge Plasma," *Phys. Plasmas* **1** (1994) 1936.

[29] *Technical Meeting and Workshop on ITER Divertor Physics Design,* ITER Joint Work Site Garching (1994).

[30] U. Samm, G. Bertchinger, P. Bogen, *et al.,* "Radiative Edges Under Control by Impurity Fluxes," *Plasma Phys. Control. Fusion* **35** (1993) B167.

[31] J. Neuhauser and the ASDEX-Upgrade Teams, "The Compatibility of High Confinement Times and Complete Divertor Detachment in ASDEX-Upgrade," *Proc. 22nd EPS Conf. on Controlled Fusion and Plasma Physics,* Bournemouth, UK (1995) 139.

[32] A. W. Leonard, S. L. Allen, M. E. Fenstermacher, *et al.,* "Radiation Distributions in Detached Divertor Operation on DIII-D," General Atomics report GA-A22068; also in *Proc. 22nd EPS Conf. on Controlled Fusion and Plasma Phys.*, Bournemouth, UK (1995).

[33] P. Yushmanov, T. Takizuka, K. S. Riedel, *et al.,* "Scalings for Tokamak Energy Confinement," *Nucl. fusion* **30** (1990) 1999.

[34] F. Perkins, P. Barabaschi, G. Bosia, *et al.,* "ITER Physics Basis", *Proc. 15th Int. Conf. on Plasma Phys. and Controlled Nucl. Fusion Research,* Seville, Spain (Sep. 1994), International Atomic Energy Agency, Vienna (1996).

[35] J. Sheffield, "Physics Requirements for an Attractive Magnetic Fusion Reactor," *Nucl. Fusion*, **25** (1985) 1733.

[36] R. J. Goldston, S. H. Batha, R. H. Bulmer, *et al.,* "Advanced Tokamak Physics–Status and Prospects," *Plasma Phys. Control. Fusion* **36** (1994) B213.

[37] S. M. Kaye and the ITER Joint Central Team and Home Teams, "Projection of ITER Performance Using the Multi-Machine L- and H-Mode Databases," *Proc. 15th Int. Conf. on Plasma Phys. and Controlled Nucl. Fusion Research,* Seville, Spain (Sep. 1994), International Atomic Energy Agency, Vienna (1996). 1994) IAEA-CN-60/E-P-3.

[38] F. Levington, M. C. Zarnstorff, S. H. Batha, *et al.,* "Enhanced Confinement with Reversed Magnetic Shear in TFTR," *Phys. Rev. Lett.* **75** (1995) 4417.

[39] E. J. Strait, L. L. Lao, M. E. Mauel, *et al.,* "Enhanced Confinement and Stability in DIII-D Discharges with Reversed Magnetic Shear," *Phys. Rev. Lett.* **75** (1995) 4420.

[40] A. Sykes, G. W. Crawford, G. Cunningham, *et al.,* "The START Spherical Tokamak," *Proc. IEEE 16th Symp. on Fusion Eng.,* Champaign, IL (Oct. 1995) IEEE No. 95CH35852, IEEE, Piscataway, NJ (1995) 1442.

[41] D. Reiter, G. Wolf, and H. Kever, "Burn Condition, Helium Particle Confinement and Exhaust Efficiency," *Nucl. Fusion* **30** (1990) 2141.

[42] R. Behrisch and V. Prozesky, "Particle and Power Exhaust for a Fusion Plasma," *Nucl. Fusion* **30** (1990) 2166.

[43] R. J. Taylor, B. D. Fried, and G. J. Morales, "Burn Threshold for Fusion Plasmas with Helium Accumulation," *Comm. Plasma Phys.* **13** (1990) 227.

[44] D. L. Hillis, K. H. Finken, J. T. Hogan, *et al.,* "Helium Exhaust and Transport Studies with the ALT-II Pump Limiter in the TEXTOR Tokamak," *Phys. Rev. Lett.* **65** (1990) 2382.

[45] D. L. Hillis, J. T. Hogan, K. H. Finken, *et al.,* "Helium Transport in Enhanced Confinement Regimes on the TEXTOR and DIII-D Tokamaks," *J. Nucl. Mat.* **196-198** (1992) 35.

[46] M. R. Wade, D. L. Hillis, J. T. Hogan, *et al.,* "Helium Exhaust Studies in H-Mode Discharges in the DIII-D Tokamak Using an Argon-Frosted Divertor Cryopump," *Phys. Rev. Lett.* **74** (1995) 2702.

[47] M. R. Wade, D. L. Hillis, J. T. Hogan, *et al.,* "Helium Transport and Exhaust Studies in Enhanced Confinement Regimes in DIII-D," *Phys. Plasmas* **2**, (1995) 2357.

[48] C. G. Bathke and the ARIES Team, "A Preliminary Systems Assessment of the Starlite DEMO Candidates," *Proc. IEEE 16th Symp. on Fusion Eng.,* Champaign, IL (Oct. 1995) IEEE No. 95CH35852, IEEE, Piscataway, NJ (1995) 1139.

[49] C. E. Kessel, "Bootstrap Current in a Tokamak," *Nucl. Fusion* **34** (1994) 1221.